FULL PAPERS

Magnetic Resonance in Medicine 62:1–10 (2009)

# Imaging Considerations for In Vivo $^{13}$C Metabolic Mapping Using Hyperpolarized $^{13}$C-Pyruvate

Y-F. Yen,[1*] S.J. Kohler,[2] A.P. Chen,[3] J. Tropp,[1] R. Bok,[4] J. Wolber,[5] M.J. Albers,[4,6] K.A. Gram,[7] M.L. Zierhut,[4,6] I. Park,[4,6] V. Zhang,[4,6] S. Hu,[4,6] S.J. Nelson,[4,6] D.B. Vigneron,[4,6] J. Kurhanewicz,[4,6] H.A.A.M Dirven,[7] and R.E. Hurd[1]

**One of the challenges of optimizing signal-to-noise ratio (SNR) and image quality in $^{13}$C metabolic imaging using hyperpolarized $^{13}$C-pyruvate is associated with the different MR signal time-courses for pyruvate and its metabolic products, lactate and alanine. The impact of the acquisition time window, variation of flip angles, and order of phase encoding on SNR and image quality were evaluated in mathematical simulations and rat experiments, based on multishot fast chemical shift imaging (CSI) and three-dimensional echo-planar spectroscopic imaging (3DEPSI) sequences. The image timing was set to coincide with the peak production of lactate. The strategy of combining variable flip angles and centric phase encoding (cPE) improved image quality while retaining good SNR. In addition, two aspects of EPSI sampling strategies were explored: waveform design (flyback vs. symmetric EPSI) and spectral bandwidth (BW = 500 Hz vs. 267 Hz). Both symmetric EPSI and reduced BW trended toward increased SNR. The imaging strategies reported here can serve as guidance to other multishot spectroscopic imaging protocols for $^{13}$C metabolic imaging applications. Magn Reson Med 62:1–10, 2009. © 2009 Wiley-Liss, Inc.**

**Key words: hyperpolarized $^{13}$C; EPSI; in vivo metabolism; 3D spectroscopic imaging; metabolic dynamics**

MR spectroscopic imaging of hyperpolarized 1-[$^{13}$C]-pyruvate (noted herein as $^{13}$C-pyruvate) is a promising technique for mapping metabolic activity in vivo, as demonstrated in recent animal studies (1–9). This method uses dynamic nuclear polarization (DNP) and a rapid in-field dissolution process to produce a highly polarized metabolic contrast agent (10). In less than 1 min following injection, $^{13}$C-pyruvate and its metabolic products 1-[$^{13}$C]-lactate (noted herein as $^{13}$C-lactate), 1-[$^{13}$C]-alanine (noted herein as $^{13}$C-alanine), and $^{13}$C-bicarbonate can be mapped at relatively high spatial resolution. This technology is especially promising in oncology, where lactate levels have been shown to correlate with disease progression (11) and response to therapy (12).

The primary goal of this study was to optimize detection signal-to-noise ratio (SNR) and image quality in metabolic images of both $^{13}$C-lactate and $^{13}$C-pyruvate in multishot acquisition. The work was focused on strategies to minimize detection and image quality limitations associated with multiple metabolites, each with very different dynamics. Previous, nonspectroscopic studies have reported flip angle and phase-encode order strategies to optimize SNR and reduce image artifacts in hyperpolarized gas imaging (13–16). The impact of image timing relative to a rapid variation of contrast medium concentration (17) has also been reported. In this work, we examined the timing and sampling strategies for spectroscopic imaging of hyperpolarized $^{13}$C-pyruvate and $^{13}$C-lactate, with a focus on the different dynamic responses of each.

Following an injection of hyperpolarized $^{13}$C-pyruvate, the in vivo pyruvate signal is typically many times larger than the lactate signal, and has a very different time course (3,4,8). Typically, the $^{13}$C-pyruvate signal increases rapidly, reaches a maximum shortly after the end of injection, and then decays, due to $T_1$ relaxation and metabolism. Lactate signal increases gradually after the injection, peaks at about 10 s after the pyruvate maximum, and reaches a quasi-steady-state (signal plateau) lasting for 12–15 s before decaying. The quasi-steady-state is the result of competing processes between lactate $T_1$ relaxation and metabolic conversion from pyruvate. Maximum lactate image SNR is obtained by sampling during the lactate signal plateau. The pyruvate signal typically varies rapidly during the lactate plateau, and thus for imaging sequences that use multiple excitations for phase encoding, the *k*-space signal will be convolved with the change in signal, and may result in image artifacts. In a recent study (9), we reported the combined use of variable flip angles (VFA) and centric phase encoding (cPE) as one strategy for reducing these artifacts in single-slice fast two-dimensional (2D) chemical shift imaging (CSI). In this work we provide simulations and animal experiments to demonstrate the advantage of this approach. A second goal of this study was to sample the metabolic process in three spatial dimensions. We explored variations of echo-planar spectroscopic imaging (EPSI) sampling strategies and applied a

[1]GE Healthcare Global Applied Sciences Laboratory, Menlo Park, California, USA.

[2]Department of Chemistry, Union College, Schenectady, New York, USA.

[3]GE Healthcare Global Applied Sciences Laboratory, Toronto, Ontario, Canada.

[4]Department of Radiology, University of California, San Francisco, San Francisco, California, USA.

[5]GE Healthcare Medical Diagnostics R&D, Amersham, UK.

[6]Joint Graduate Group in Bioengineering, University of California, San Francisco/University of California, Berkeley, San Francisco, California, USA.

[7]GE Healthcare Medical Diagnostics R&D, Oslo, Norway.

*Correspondence to: Yi-Fen Yen, GE Healthcare, 333 Ravenswood Ave., Building 307, Menlo Park, CA 94025, USA. E-mail address: yi-fen.yen@ge.com

Received 30 December 2007 ; revised 7 January 2009; accepted 11 January 2009.

DOI 10.1002/mrm.21987

Published online 24 March 2009 in Wiley InterScience (www.interscience.wiley.com).

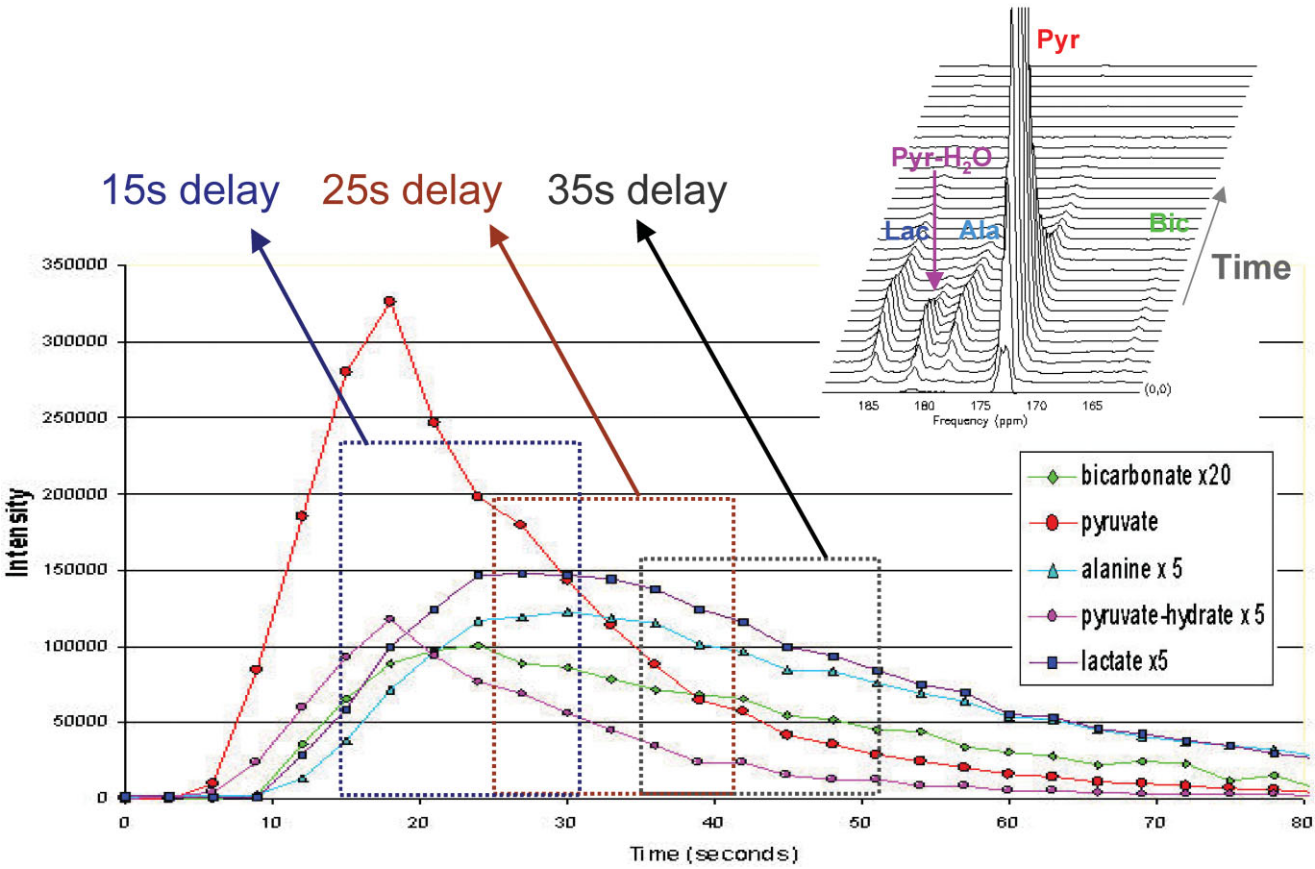


FIG. 1. Signal-time courses derived from dynamic $^{13}$C MR spectra acquired on a rat following an injection of hyperpolarized $^{13}$C-1-pyruvate (4). The acquisition parameters were 5 kHz, 2048 points, 5° flip angle, and 3-s temporal resolution. The insert plot shows the changes of spectra over time for lactate, pyruvate-hydrate, alanine, pyruvate, and bicarbonate peaks (from left to right). The three boxes illustrate the time window of a typical 17-s fast CSI acquisition at three different time delays: 15 s, 25 s, and 35 s.

gridding technique to include samples acquired during both forward and return passage of EPSI in order to improve the SNR while keeping the 5-mm spatial resolution, 16-Hz spectral resolution, and total scan time the same. These sampling strategies were evaluated on rats and compared with theoretical expectations.

## MATERIALS AND METHODS

### VFA, Imaging Window, and cPE

The VFA technique uses a series of progressively increasing flip angles up to 90° in multiple excitations. The technique has been elegantly applied to hyperpolarized noble gas imaging (13–16) in order to utilize all longitudinal magnetization and maximize the SNR. When $T_1$ is known, the design of VFA incorporates the $T_1$ value and yields constant transverse magnetization at each excitation, preventing $T_1$ modulation of the signal of different phase encode lines. For this work, the $T_1$ of $^{13}$C-pyruvate solution is about 60 s ex vitro but the $T_1$'s of $^{13}$C metabolites in vivo are difficult to measure because of the competing metabolic processes. We designed the VFA based on the constant level of lactate signal plateau observed in the dynamic study. This is legitimate for lactate when the acquisition coincides with its signal plateau (Fig. 1). Then the flip angle of the $n$th excitation, $\theta_n$, is expressed as

$$\theta_n = tan^{-1}(sin(\theta_{n+1})), \quad [1]$$

where the flip angle of the last excitation is 90°. For phase encoding matrixes of 12 × 12 and 16 × 16, the VFA starts from 4.8° and 3.6°, respectively.

Figure 1 shows an example of dynamic curves acquired on a rat following an injection of hyperpolarized $^{13}$C-pyruvate from a previous study (4). A 5° flip angle was applied and an free induction decay (FID) of 2048 points over a 5-kHz spectral bandwidth (BW, spectral resolution = 2.4 Hz) was collected every 3 s. The dynamic scan and injection started at the same time. The spectra in Fig. 1 show the chemical shifts of pyruvate and its metabolic products. The three boxes in Fig. 1 illustrate a fast CSI acquisition window of 17 s at three time delays: 15 s, 25 s, and 35 s from the start of injection. When applying the VFA design as described above and a time delay of 25 s, we expect to obtain a fairly constant transverse magnetization for lactate, and decreasing signal for pyruvate from excitation to excitation. Consequently, the order of phase encoding should have little effect on the signal and image quality of lactate but significant effect on those of pyruvate. Some tradeoff between SNR and image quality is expected.

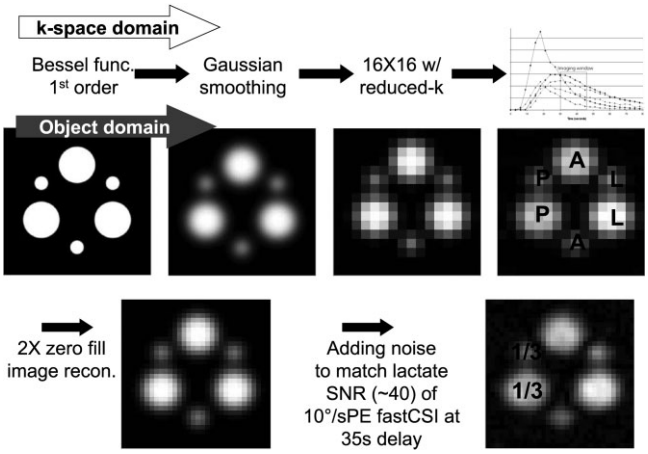


FIG. 2. Schematic diagram to illustrate the *k*-space simulation of fast CSI acquisition using Bessel functions of the first order, smoothed by a Gaussian filter, and then sampled by a 16 × 16 matrix, with 20% reduction in *k*-space corner coverage. The corresponding images at each step of the *k*-space simulation are shown here under "Object domain." The intensity of pyruvate circles is scaled down by a factor of three in all simulation images presented in this work so that lactate and alanine circles can be easily seen in the images.

### Mathematical Simulation of 2D Fast CSI

Mathematical simulations were performed using dynamic data from rats to model the dynamic behavior of pyruvate and lactate. The impact of imaging time window, variation of flip angles, and order of phase encoding on SNR and image quality were simulated for fast CSI sequence. This sequence (4) employed multiple excitations, each followed by phase encoding gradients, data acquisition, and spoiling gradients at the end of the readout. The repetition time was minimized (TR = 84 ms) and the corners of *k*-space were not sampled in order to reduce the total scan time.

Three pairs of circles were simulated, each consisting of a large circle (10-mm radius) and a small circle (3.75-mm radius) to mimic various organ or tumor sizes in animals. *k*-Space data were simulated for fast CSI 2D acquisition by creating these circular phantoms using Bessel functions of the first order, smoothed by a Gaussian filter of 1.07 cycles/pixel (i.e., full-width half-maximum = 214 cycles/m), and then sampled by a 16 × 16 matrix, with 20% reduction of *k*-space coverage at the corners. A field of view (FOV) of 80 mm × 80 mm was used, resulting in a nominal resolution of 5 mm × 5 mm. The purpose of the Gaussian filter was to smooth the sharp edge of the simulated phantoms slightly to get rid of Gibb's ringing after sampling. Without smoothing, sharp phantoms sampled with very few pixels (4 × 4 pixels for the large circles) would yield severe Gibb's ringing and make it difficult to evaluate the SNR within the phantoms. Figure 2 shows the corresponding images at each step of the *k*-space simulation. The in vivo dynamic data of pyruvate (P), lactate (L), and alanine (A), corrected for the successive 5° flip angles, were applied to the three pairs of circles to mimic the in vivo signal (Fig. 2). Finally, complex random noise was added to the *k*-space data such that the simulated lactate SNR matched that of rat kidney acquired in vivo by using fast CSI with a constant 10° and sequential phase encoding (sPE) order. The same noise level was then used in all simulations. cPE was implemented by prioritizing the order of sampling points according to their distances (1/cm) to the origin of *k*-space. This sorting method allows a more concentric sampling pattern in *k*-space even if the FOV is anisotropic.

The simulation images were reconstructed by zero-filling *k*-space to 32 × 32 before Fourier transformation was applied. Signal was obtained by averaging a 7.5-mm × 7.5-mm area at the center of each large circle. Noise was calculated as the standard deviation of all voxels in a noise image, constructed by using only the complex random noise. The image quality was assessed by the broadening of point spread functions (PSFs). Simulations were performed to compare SNR and image quality at three time delays: 15 s, 25 s, and 35 s; two phase encoding orders: sPE and cPE; and two flip angle schemes: constant 10° vs. VFA. Additional simulations were performed to evaluate the SNR advantage of VFA when compared with a range of constant flip angles.

### 3DEPSI Sampling Strategies

3D spectroscopic imaging can be rapidly acquired by using 3DEPSI types of sequences, which typically employ multiple excitations, each followed by phase encoding gradients and an EPSI gradient (9,18–21). The efficiency of EPSI waveform design is characterized as the ratio of the data collection period to the total period of the EPSI waveform. Flyback EPSI (20,21) interleaves frequency-encoding gradients with large rewind (or flyback) gradients to refocus the transverse magnetization rapidly during the data acquisition. It typically uses data collected during the plateau of encoding gradients for image reconstruction and does not acquire data with the rewind gradients. Although not as efficient as the fully-sampled EPSI, flyback-EPSI is an efficient compromise for proton imaging because of its large gyromagnetic ratio and, hence, only a small fraction of time spent on rewind gradients. But flyback EPSI is much less efficient for $^{13}C$ imaging. For 5-mm spatial resolution and 500-Hz spectral BW in $^{13}C$ with 40 mT/m gradient amplitude and 150 T/m/s slew rate, flyback EPSI (Fig. 3; top) has an efficiency of only 46%. To increase the efficiency for $^{13}C$, one would have to utilize higher performance gradients, decrease the spatial resolution, or reduce the spectral BW. Here we tested a flyback EPSI waveform of a reduced spectral BW to 267 Hz (Fig. 3; bottom). In addition, we explored the utility of a fully-sampled symmetric EPSI (Fig. 3; middle) designed for 5-mm resolution and 500-Hz BW in $^{13}C$. These two EPSI waveforms were tested against flyback EPSI of 500 Hz in terms of sampling efficiency, SNR, and image qualities in 3D hyperpolarized $^{13}C$ metabolic imaging of rats.

### Animal Experiments

*Experiment A: VFA/cPE in 2D Fast CSI*

The imaging strategies of VFA/cPE and 10°/sPE were compared on two rats using fast CSI at a 25-s time delay. Each rat received three injections. The imaging strategies are listed in Table 1a. A 10-mm axial slice was prescribed on

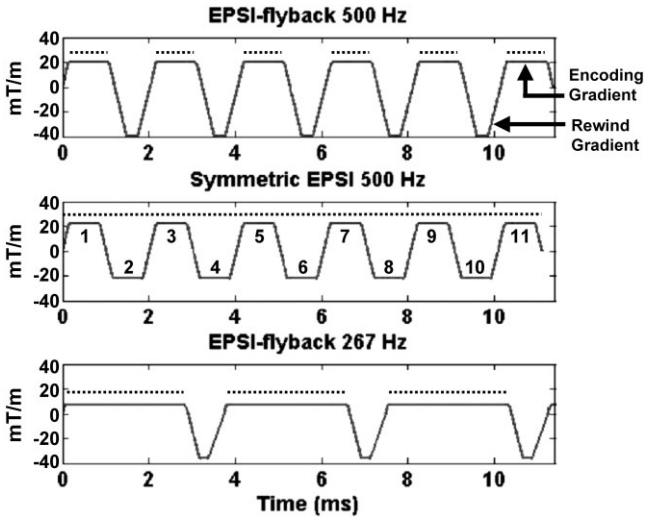


FIG. 3. Gradient waveforms evaluated in this work: flyback EPSI at 500 Hz (top), symmetric EPSI at 500 Hz (middle), and flyback EPSI at 267 Hz (bottom). The flyback EPSI waveform consists of cycles of encoding and rewind gradients (as labeled). The symmetric EPSI waveform consists of odd and even echoes (as numbered). The dashed lines indicate the period at which data were collected for reconstruction.

the rat in supine position to include at least one kidney. The imaging matrix size = 16 × 16, FOV = 80 mm × 80 mm, spectral BW = 5 kHz, time points = 256 (spectral resolution = 19.5Hz), and TR = 84 ms. *k*-Space coverage was reduced by 20%. Total scan time was 17 s.

*Experiment B1: VFA/cPE in 3DEPSI*

We compared the VFA/cPE strategy to 10°/sPE in 3D imaging on three rats by using flyback 3DEPSI at BW = 500 Hz. A 40-mm axial slab was excited to cover both kidneys. The EPSI train was applied in the right-left direction. Twelve phase encodings were applied in each of the anterior-posterior (A/P) and superior-inferior (S/I) directions. The matrix size = 18 × 12 × 12, FOV = 90 mm ×60 mm × 60 mm, spectral BW = 500 Hz, time points = 32 (spectral resolution = 15.6Hz), TR = 90 ms, and total scan time = 13 s.

*Experiment B2: Reduced Spectral BW*

The flyback EPSI with reduced spectral BW allows more time for the frequency-encoding gradients to play out while keeping the same maximum flyback gradients and, hence, improves the flyback EPSI efficiency. The tradeoff is spectral aliasing. The $^{13}$C MR spectrum consists of pyruvate, lactate, alanine, and pyruvate-hydrate peaks, spread sparsely over 480 Hz at 3T, and a bicarbonate peak at about –700 Hz from lactate (Fig. 1; inset). At BW = 267 Hz and the center frequency close to alanine, aliasing is such that both lactate and pyruvate peaks wrap in, the three major peaks (lactate, alanine, and pyruvate) are about equally spaced, and pyruvate-hydrate and pyruvate peaks overlap. The latter elevates the total pyruvate signal with no downside as pyruvate-hydrate is not metabolically active and is in rapid exchange with pyruvate. The bicarbonate peak wraps in and overlaps with alanine peak. This could be a drawback for applications that are concerned about bicarbonate or alanine signals. A flyback EPSI of BW = 267 Hz and resolution = 5 mm was evaluated on four rats (Table 2) with VFA/cPE. All other imaging parameters are the same as those in Experiment B1.

*Experiment B3: Symmetric EPSI*

A fully-sampled symmetric EPSI waveform allows us to utilize the hardware limit in order to obtain either the maximum spectral BW or maximum spatial resolution. Using the maximum gradient amplitude = 40 mT/m and maximum slew rate = 150 T/m/s, a maximum spectral BW = 670 Hz can be achieved with a spatial resolution = 5-mm. Or, a maximum resolution = 3.3 mm can be obtained with a spectral BW = 500 Hz. In this experiment, a symmetric EPSI of BW = 500 Hz and resolution = 5-mm was evaluated on four rats with VFA/cPE (Table 2). All other imaging parameters are the same as those in Experiment B1.

## MR Hardware and RF Coils

The animal experiments were performed on a GE Signa Excite 3T clinical scanner. A custom-built dual-tuned $^{1}$H/$^{13}$C coil was used for RF transmission and signal reception (22). The proton coil is linear and the carbon coil is a quadrature birdcage design. The transmit $B_1$ of carbon coil is homogeneous within an area of 9 cm in length (S/I direction) and 7.5-cm diameter in-plane (axial).

Table 1
a. SNR of Fast CSI Data Acquired on Two Rats Using Two Imaging Strategies*

| Rat | Imaging strategies | Polarization (%) | nSNR_Lac | nSNR_Pyr |
|---|---|---|---|---|
| 1 | VFA/cPE | 25.7 | 59.6 | 312.0 |
| 1 | VFA/cPE | 26.3 | 47.5 | 276.0 |
| 1 | 10°/sPE | 21.0 | 39.7 | 168.1 |
| 2 | 10°/sPE | 24.4 | 42.6 | 132.1 |
| 2 | 10°/sPE | 21.3 | 46.1 | 125.4 |
| 2 | VFA/cPE | 19.0 | 59.9 | 203.0 |

b. Average SNR of Lactate and Pyruvate for the Two Imaging Strategies and SNR Enhancement Factors†

| | ave_SNR_Lac | ave_SNR_Pyr |
|---|---|---|
| VFA/cPE | 55.7 | 263.6 |
| 10°/sPE | 42.8 | 141.8 |
| SNR enhancement | 1.3 | 1.9 |
| Expected enhancement | 1.7 | 2.6 |

*The percentage polarization listed is the liquid state polarization. SNR was extracted from the left kidney of rats and then normalized by its liquid state polarization to 20% (arbitrarily chosen) to remove the variability due to different polarization in each acquisition.
†On average, the SNR of lactate was enhanced by a factor of 1.3 and pyruvate by a factor of 1.9 by applying VFA/cPE as compared to 10°/sPE. The expected enhancement factors from the simulations are also listed.
nSNR = normalized SNR, Lac = lactate, Pyr = pyruvate, VFA = variable flip angle, cPE = centric phase encoding, 10° = constant 10° flip angle, sPE = sequential phase encoding, ave_SNR = average SNR.

Table 2
a. SNR of 3DEPSI Data Acquired on Four Rats*

| Experiment | Strategies | lk SNR | Pol (%) | nSNR | lk SNR | Pol (%) | nSNR | lk SNR | Pol (%) | nSNR | lk SNR | Pol (%) | nSNR |
|---|---|---|---|---|---|---|---|---|---|---|---|---|---|
| 0 | fb 500 VFA/cPE | 14.5 | 22.1 | 13.11 | 9.0 | 19.5 | 9.21 | 11.2 | 26.5 | 8.43 | 13.5 | 21.6 | 12.54 |
| 1 | fb 500 10°/sPE | 10.6 | 20.4 | 10.68 | 8.6 | 24.1 | 7.13 | 7.7 | 17.2 | 8.99 | N/A | N/A | N/A |
| 2 | fb 267 VFA/cPE | 16.5 | 21.2 | 15.58 | 12.4 | 22.2 | 11.14 | 10.8 | 20.9 | 10.40 | 18.3 | 21.5 | 17.00 |
| 3 | sym 500 VFA/cPE | 19.0 | 21.8 | 17.38 | 14.0 | 22.9 | 21.28 | 13.1 | 23.0 | 11.39 | 16.7 | 19.3 | 17.37 |

b. SNR Enhancement Factor Calculated With Respect to the SNR of 500-Hz fb-EPSI Experiment Using the VFA/cPE Strategy

| Experiment | Strategies | SNR Enhancement Factor | | | | | Expected |
|---|---|---|---|---|---|---|---|
| | | Rat 1 | Rat 2 | Rat 3 | Rat 4 | Average | |
| 0 | fb 500 VFA/cPE | 1 | 1 | 1 | 1 | 1 | |
| 1 | fb 500 10°/sPE | 0.79 | 0.77 | 1.07 | N/A | 0.88 | 0.74 |
| 2 | fb 267 VFA/cPE | 1.19 | 1.21 | 1.23 | 1.36 | 1.25 | 1.28 |
| 3 | sym 500 VFA/cPE | 1.33 | 1.33 | 1.35 | 1.38 | 1.35 | 1.36 |

*Four EPSI strategies were tested on each rat, except for Rat 4. The Pol is listed for each experiment. SNR was extracted from lactate lk SNR and then nSNR was calculated to 20% polarization for comparisons.
SNR = signal-to-noise ratio, 3DEPSI = three-dimensional echo-planar spectroscopic imaging, Pol = liquid state polarization, lk SNR = left kidney SNR, nSNR = normalized SNR, fb = flyback, sym = symmetric, VFA = variable flip angle, cPE = centric phase encoding, 10° = constant 10° flip angle, sPE = sequential phase encoding.

### Animal Preparation

Sprague-Dawley rats of 230–500 g body weight were used for the imaging study. Animals underwent general anesthesia by isoflurane (2%–3%) inhalation. After rats were transported to the MRI scanner, anesthesia continued by delivering isoflurane (1%–2%) at 0.5 to 1.0 liters/min via a long tube to a cone placed over the rat's nose and mouth. The rats were placed on a heating pad inside a rat coil to maintain a body temperature of 37°C during the study. The blood oxygen saturation, heart rate, and respirations rate were monitored continuously. Hyperpolarized $^{13}$C-pyruvate solution was injected via a tail vein catheter. The rats used in Experiment A received three injections, each of ~3 ml and the rats used in Experiments B1–B3 received four injections, each of 1.1 ml. The injection duration was 12 s at an interval of about 1.5 h. Three to four injections were administered in an animal over 5 to 6 h. Following the completion of image acquisitions, the rats were euthanized. All procedures followed the protocol approved by the University of California, San Francisco Institutional Animal Care and Use Committee.

### Polarization Technique

Samples consisting of $^{13}$C-1-pyruvic acid and trityl radical mixture were polarized by the DNP technique. The time constant of the solid-state polarization build-up was about 14 min and it took 70 to 80 min to fully polarize a sample. The dissolution procedure has been described elsewhere (10). The dose concentration was 79 mM, which was obtained by dissolving 44 mg $^{13}$C-1-pyruvic acid/trityl mixture in 6.06 ml of trishydroxymethylaminomethane (TRIS)/ethylene diamine tetraacetic acid (EDTA)/NaOH dissolution medium. The time from the sample dissolved to the start of injection was about 20 s. A small amount (0.5–1 ml) of the dissolved pyruvate solution was withdrawn about 10 s after the sample dissolved for liquid-state polarization measurement using a low-field NMR spectrometer (polarimeter). The percentage polarization was calibrated, prior to the animal studies, by simultaneous measurements in the MRI system and the polarimeter. The polarization ranged from 17.2% to 26.5%. The pH varied from 7.2 to 8.0.

### MRI Protocol

For proton imaging, transmit gain (TG) was determined by a standard automatic prescan protocol. A proton localization scan was performed in three planes, followed by three $T_2$ fast spin-echo (FSE) high-resolution scans, one for each orientation. For $^{13}$C imaging, the TG was adjusted manually using a bottle of corn oil prior to placing the animal in the scanner. The TG of the RF coil was not sensitive to variations in loading (22). The $^{13}$C imaging prescription was based on the $T_2$-FSE images. The $^{13}$C imaging protocols are described earlier. A 5-ml syringe filled with ~2 ml of 1.77 M, 20% sodium $^{13}$C-1-lactate (Cambridge Isotope Laboratories) was placed on top of the rat within the FOV as a reference.

### MR Data Reconstruction and Analysis

All data reconstruction and analysis were performed by using custom programs in Matlab (The MathWorks, Inc., Natick, MA, USA). The fast CSI rat data were zero-filled to $32 \times 32$ in the spatial-frequency domains. No zero-fill was applied to the time-domain. No apodization was applied to any domain. The maximum magnitude of each metabolite peak was used to construct individual metabolite maps.

For the flyback EPSI data analysis, zero-fill was applied to right/left (R/L) and anterior/posterior (A/P) directions but no zero-fill was applied in the S/I direction or in the time domain. The final matrix size was 32 (time) × 64

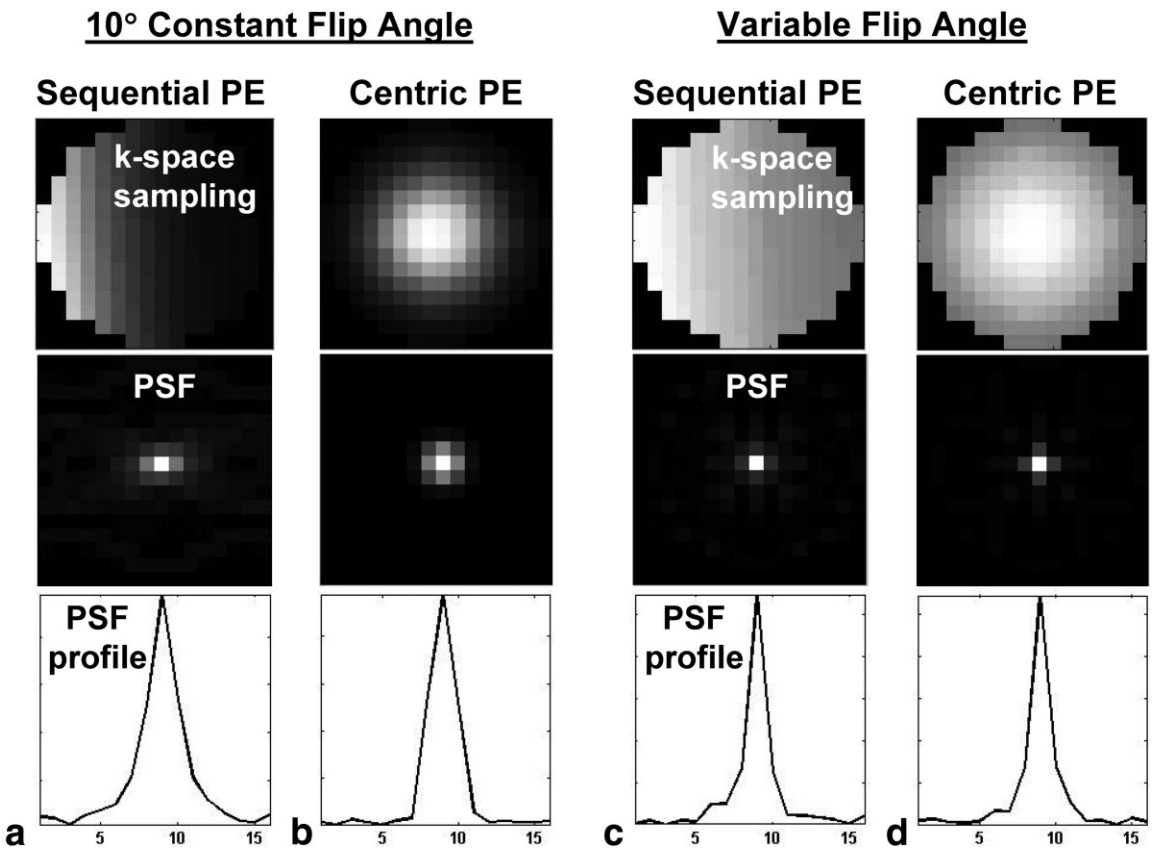


FIG. 4. Simulated data for a constant 10° flip angle and VFAs in sequential vs. centric phase encoding orders based on the fast CSI acquisition of a 16 × 16 matrix. The signal intensity in *k*-space (*ky* vs. *kz*; top row) was extracted from the pyruvate dynamic curve (Fig. 1; red) at a 25-s time delay. The corresponding PSFs (center row) and their profiles (bottom row) plotted horizontally across the center of the matrix are shown to predict the severity of image blurring. The PSF profiles of the constant flip angle schemes are both broader than those of the VFA schemes, indicating that image blurring is expected to be more severe with a constant flip angle. The profile of the VFA/sPE strategy is very similar to but perhaps slightly sharper than the profile of the VFA/cPE strategy.

(R/L) × 32 (A/P) × 12 (S/I). For the symmetric EPSI data analysis, a gridding algorithm was applied to properly correct for relative phase among samples in *kx* vs. time domain using the designed symmetric EPSI trajectory as a weighting function. Data were then zero-filled to 32 (time) × 64 (R/L) × 32 (A/P) × 12 (S/I) prior to Fourier transformation.

Magnitude images of peak lactate and peak pyruvate were displayed and used for SNR analysis. The maximum signal of a 5-mm × 5-mm area on the left kidney was used for SNR calculations. Noise was calculated as the standard deviation of a large region (~70 mm × 50 mm) on a magnitude image displayed at a chemical shift frequency away from any metabolite peaks. The SNR was then normalized (nSNR) by its liquid state polarization to 20% (arbitrarily chosen) to remove the variability due to different polarization in each acquisition.

## RESULTS

### Simulation

The fast CSI simulation using the in vivo pyruvate dynamic signal yields expected signal distribution in *k*-space for the four imaging strategies (Fig. 4a–d; top). The corresponding PSFs and their profiles are shown in Fig. 4 to illustrate the image blurring anticipated for each scenario. Images acquired with VFA are expected to be less blurry, as suggested by the narrower PSF profiles. For all scenarios, image blur is expected to be less severe for lactate and alanine (not shown) because their dynamic signals are relatively flat during the imaging window.

Mugler (14) showed that when the longitudinal magnetization is depleted only by the RF pulses, the optimal flip angle for constant flip angle and sPE acquisition is about 5° to 7° for 140 to 260 RF excitations. Therefore, we also did fast CSI simulations from 3° to 10° constant flip angles with sEP and the results are shown in Fig. 5a. The VFA/cPE strategy is less advantageous when compared to sPE with a constant flip angle of 5° to 7° when compared to 10°/sPE. The PSF of sPE and the 6° constant flip angle (Fig. 5b) approaches the PSF of VFA/cPE, implying that the image quality should be comparable. Nevertheless, these simulations (Fig. 5) were performed retrospectively and compared to the 10° constant flip angle that was used in our experiments. The rest of the report shows the 10° constant flip angle simulation and experimental results.

Reconstructed simulation data using 10° flip angles at three time delays are shown in Fig. 6. Note that the pyru-

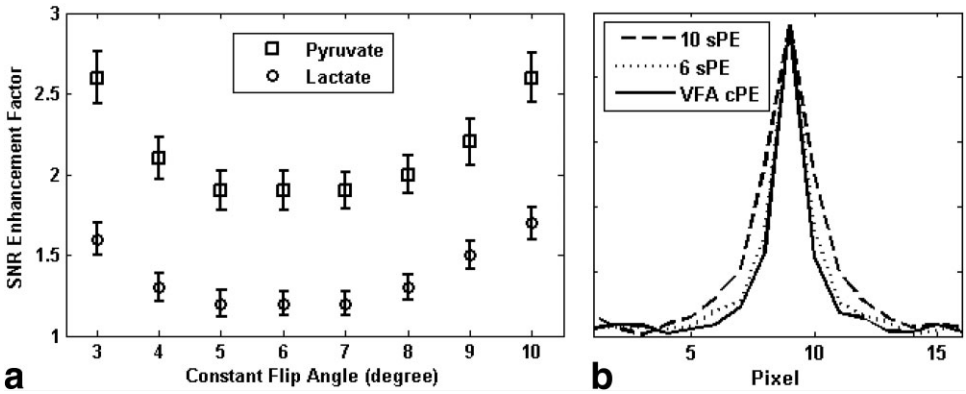


FIG. 5. **a:** SNR enhancement factor of VFA/cPE compared to sPE with a constant flip angle ranging from 3° to 10°. **b:** PSF of 10°/sPE (dashed line), 6°/sPE (dotted line), and VFA/cPE (solid line).

vate signal is scaled down by a factor of 3 so that lactate and alanine circles can be easily seen in the images. The quoted pyruvate SNR is also scaled by one-third. The early imaging window (15 s) yielded very large pyruvate signal but less lactate and alanine signals. At a 25-s delay and with cPE, the lactate SNR is high but the image is blurry in both dimensions (as is also indicated by the corresponding PSF in Fig. 4). Overall, the SNR is higher with cPE than with sPE.

Using VFA, the images are less blurry (Fig. 7) compared to the constant flip angle counterparts (Fig. 6). The pyruvate SNR is the better with cPE than with sPE at any time delay, as expected. The best lactate SNR is expected at a 25-s delay, either using sPE or cPE. At a 25-s delay, the best image quality was observed for VFA/sPE (Fig. 7). Although slightly inferior in image quality, the VFA/cPE strategy yielded much better pyruvate SNR than VFA/sPE without compromising the lactate SNR. We think the best strategy overall is the combination of VFA and cPE with an acquisition window delayed to coincide with lactate signal plateau. This strategy is also expected to work the best for 3DEPSI acquisitions.

## Animal Experiments

*Experiment A: VFA/cPE in 2D Fast CSI*

The liquid state polarization (Pol) and normalized SNR (nSNR) extracted from the left kidneys are listed in Table 1a. The VFA/cPE enhances the lactate SNR by a factor of 1.3 and pyruvate SNR by a factor of 1.9 as compared to the 10°/sPE strategy (Table 1b). However, the enhancement factors are smaller than the simulation predictions. In-flow effect may be the main cause of this discrepancy; we will discuss this below.

*Experiment B1: VFA/cPE in 3D Imaging*

The VFA/cPE strategy was compared to 10°/sPE in 3D imaging on rats using flyback EPSI of 500-Hz BW. Figure 8 shows an example of four 3DEPSI acquisitions performed on the same rat using the four sampling strategies described in Materials and Methods. The lactate SNR of the left kidney (lk_SNR) is listed in Table 2a for all the 3DEPSI data. The SNR enhancement factor (Table 2b) was calculated as the ratio of nSNR relative to the VFA/cPE data. The 10°/sPE strategy was only tested on three of the four rats due to operational error of the polarizer. The 10°/sPE SNR is 88% of the VFA/cPE SNR, larger than the prediction from simulation (74%). Similar to the discrepancy found in Experiment A, this may be due to in-flow effect.

*Experiment B2: Reduced Spectral BW*

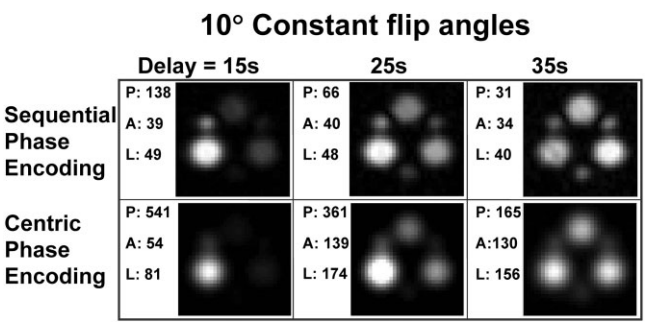


FIG. 6. Reconstructed simulated images using constant 10° flip angles at three time delays (15 s, 25 s, and 35 s) are shown here with the estimated SNR for pyruvate (P), alanine (A), and lactate (L). Note that the quoted pyruvate SNR has been scaled down by a factor of 3. The highest lactate SNR is expected with 25-s delay and cPE, but the image is blurry in both dimensions. Images of sPE are sharper but the SNRs are low for all metabolites.

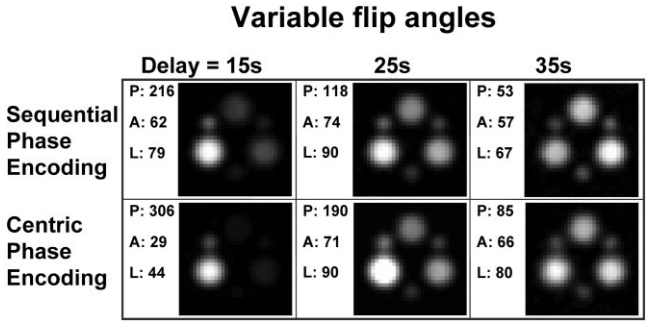


FIG. 7. Using VFA, the best lactate SNR is expected at a 25-s delay. Because the plateaus of lactate and alanine are fairly broad (~12 s), when sampling on the plateaus, similar SNRs are obtained no matter which PE order is applied. The pyruvate SNR, however, is the best with cPE. Although the image of VFA/sPE may be slightly better than the image of VFA/cPE, considering the SNR of all metabolites, the best strategy is the combination of VFA and cPE.

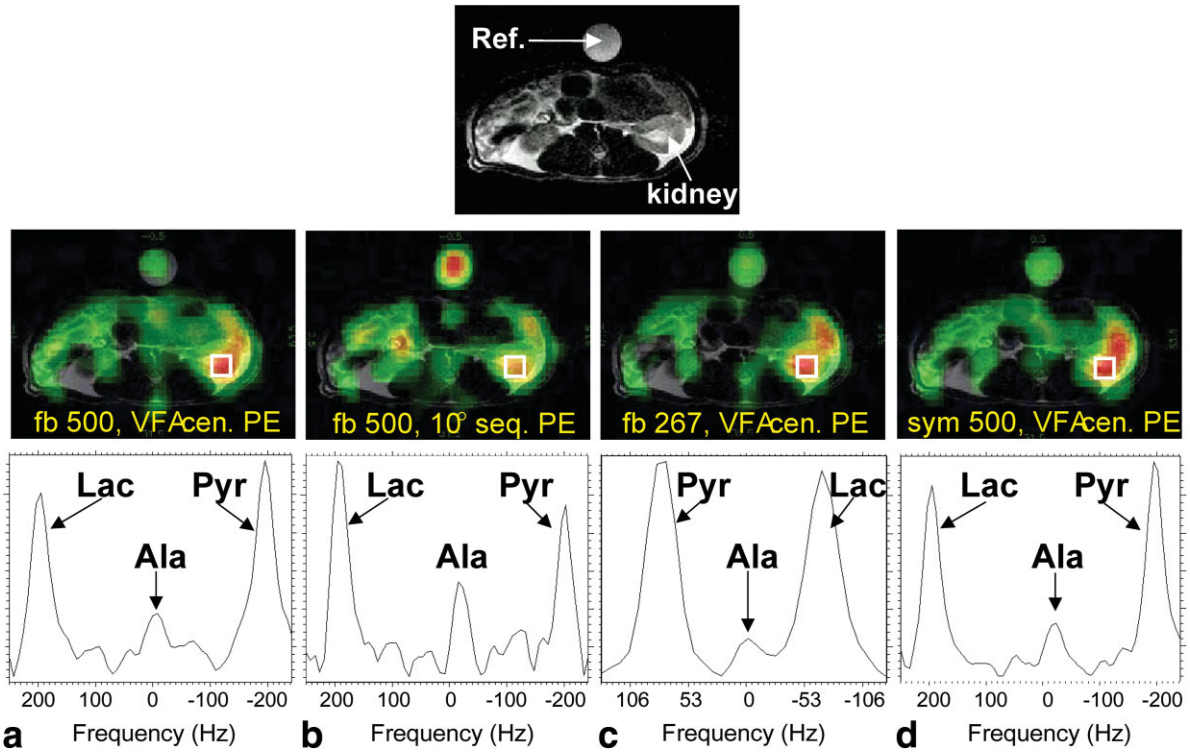


FIG. 8. Axial in vivo $^{13}$C lactate images (color) acquired by using 3DEPSI on the same rat to compare the image quality and SNR of (**a**) flyback EPSI, 500 Hz, VFA, cPE; (**b**) flyback EPSI, 500 Hz, 10° flip angles, sPE; (**c**) flyback EPSI, 267 Hz, VFA, cPE; and (**d**) symmetric EPSI, 500 Hz, VFA, cPE. The order of imaging acquisition was (a)-(d)-(c)-(b) and the same order applied for all four rats. For each data set, the spectrum obtained from a 5 mm × 5 mm area on the left kidney (white box) is shown at the bottom. The reference is a syringe filled with 1.77 M 1-$^{13}$C-lactate solution placed on the top of rat. The scan time was 13 s for each acquisition. The acquired spatial resolution was 5-mm isotropic and zero-fills were applied to generate the color metabolite maps. See Materials and Methods section for the acquisition parameters and reconstruction method. The brightest lactate signal appears in the left kidney. Strong lactate signal is also found posterior (on the top) of the left kidney on a structure that is possibly the spleen or pancreas.

When the EPSI spectral BW is reduced to 267 Hz, both the lactate and pyruvate peaks are aliased (Fig. 8c) and need to be unwrapped in the image reconstruction to ensure the pyruvate and lactate signals fall back to the correct spatial location. Figure 8c shows the distribution of lactate signals (color) consistent with that of other acquisitions on the same rat. The efficiency of the 267-Hz flyback EPSI and the 500-Hz flyback EPSI is 75% and 46%, respectively. Therefore, the SNR gain is expected to be 1.28 ($= \sqrt{0.75/0.46}$). The rat data show an average SNR enhancement of 1.25 (Table 2b), consistent with the theoretical prediction.

*Experiment B3: Symmetric EPSI*

The quality of the lactate image is good (Fig. 8d). The efficiency of symmetric EPSI is estimated to be 85% when weighing the ramp samples by the sampling density. Therefore, the symmetric EPSI waveform is expected to gain a factor of 1.36 ($= \sqrt{0.85/0.46}$) in SNR when compared with flyback EPSI of the same spatial resolution and spectral BW. The rat data yielded an average SNR enhancement of 1.35 (Table 2b), consistent with the theoretical expectation.

## DISCUSSION

This work focused on strategies to optimize lactate image quality and SNR while retaining those of pyruvate for multishot acquisitions. First, the strategy was based on an imaging acquisition window delayed to coincide with the lactate signal plateau. Second, sampling of the lactate signal was optimized by applying VFA. The VFA was designed based on the observed constant level of lactate over the imaging window. Therefore, no assumptions were required with respect to the balance of $T_1$ and metabolic activity that created the lactate plateau. Under these conditions, the choice of phase encoding order should not affect the lactate SNR, as demonstrated by the simulation. For pyruvate, the dynamic signal decreases during the typical imaging window and, hence, the cPE strategy yielded better pyruvate SNR than sPE. With a very slight compromise in image quality but an overall good SNR, VFA/cPE was chosen to be the best strategy for multishot acquisitions based on the simulation and in vivo rat data of this work. This strategy has also been applied on dog prostate $^{13}$C imaging using clinical coils and the 3D flyback EPSI sequence presented here, yielding good image quality and SNR of dog prostate (8). Although this work focused on lactate, the same strategy can be applied to alanine, which may be of interest for liver disease applications.

The appropriate time delay depends on the period of bolus injection and blood circulation time to the organ of interest. In addition, the metabolic exchange rate is higher at lower dose concentration (23) and, therefore, the lactate signal tends to reach a plateau earlier, at lower doses. Our

experience with repeated dynamic scans is that the timing of lactate signal is fairly reproducible, as long as the injection method, dose concentration, the imaging organ, and the animal species are the same. Therefore, it is reasonable to use a priori timing information from a separate experiment to determine the appropriate time delay. However, when imaging organs in disease conditions, one should acquire dynamic information on the diseased organ and should not assume the uptake kinetics are the same as the normal organ.

Since the 3DEPSI protocol was not randomized, alternation of pyruvate metabolism over several hours of isoflurane anesthesia may be a concern for systematic errors. In a different study (not shown) where repeated measurements were performed three times in each of two rats with identical acquisition parameters, no systematic trend was found in lactate/pyruvate or alanine/pyruvate ratios during 6-h anesthesia sessions, and the intrasubject variability was 15% to 20%. In a recent dog study (8) with multiple large-dose $^{13}C$-pyruvate injections, blood samples drawn shortly before and after each pyruvate injection were analyzed for the amount of pyruvate and lactate in blood. The results (not shown here) indicated that pyruvate metabolism is rapid and no cumulative effect is expected at intervals of 1.5 h. The dose per kg of body weight used in the dog study is comparable to the 3-ml doses used in the rats in this study.

The SNR enhancement using VFA/cPE was found to be consistently low compared to the theoretical predictions. This discrepancy is likely due to in-flow effect. The simulation did not take into account the signal change due to in-flow for different flip angles used for imaging.The VFA for a 12 × 12 matrix in 3DEPSI started at 4.8° and then increased very slowly, with at least three-quarters of the excitations less than 10°. Therefore, compared to the constant 10° acquisition, the additional signal contribution from in-flow would be less in the VFA acquisition. This may explain the decrease of the advantage of VFA/cPE as compared to 10°/sPE. For the fast CSI acquisition, 204 excitations were performed, and one may expect an even larger discrepancy compared to the theoretical prediction. The trend in our data indicated the same: the SNR enhancement measured in fast CSI was only about 76% (=1.3/1.7 for lactate) of the enhancement predicted by simulation, whereas in 3DEPSI, it was 84% (=0.74/0.88). Another factor is the accuracy of the flip angle calibration. However, this would affect both the VFA and constant flip angle measurements and the effect is expected to be smaller than the in-flow effect.

Symmetric EPSI improved the lactate SNR by 35% compared to the flyback EPSI. There is no problem combining the odd- and even-echo data when the data are properly gridded on the *kx* vs. time domain. The effect of eddy currents is expected to be insignificant in this work because for 5-mm resolution, the waveform amplitude was 2.2 mT/m, much less than the maximum 40 mT/m. The close agreement between the theoretical and measured SNR enhancement factors further demonstrates this. For future imaging studies utilizing full gradient strength and slew-rate, it is advisable to use the measured trajectories in data gridding to eliminate potential image artifacts. The symmetric EPSI has other advantages. Bicarbonate, a metabolic byproduct, as pyruvate, enters the tricarboxylic acid cycle, has a chemical shift of about 700 Hz from lactate at 3T. With a spatial resolution of 5.6 mm and 720-Hz spectral BW, it is possible to capture the bicarbonate peak by using symmetric EPSI. It is also possible to use odd and even echoes separately in order to gain spectral BW. However, $N/2$ aliasing peaks may appear due to uncertainties of waveform timing, eddy current effects and $T_2$*. The potential of symmetric EPSI for $^{13}C$ imaging is worth exploring further.

## CONCLUSIONS

Hyperpolarized $^{13}C$ imaging using variable flip angles and cPE at an appropriate time delay yielded good SNR and image quality of pyruvate and lactate, as demonstrated here in simulation and rat experiments using 2D fast CSI and 3DEPSI. In addition, two aspects of EPSI sampling strategies were explored: waveform design (flyback vs. symmetric EPSI) and spectral BW (500 Hz vs. 267 Hz). Both yielded increased SNR, up by 35% from symmetric EPSI and 25% from reduced BW. The imaging strategies reported here can be applied to other multishot acquisitions for hyperpolarized $^{13}C$ metabolic imaging applications.

## REFERENCES


1. Golman K, in't Zandt R, Lerche M, Pehrson R, Ardenkjaer-Larsen JH. Metabolic imaging by hyperpolarized $^{13}C$ magnetic resonance imaging for in vivo tumor diagnosis. Cancer Res 2006;66:10855–10860.
2. Golman K, Petersson JS. Metabolic imaging and other applications of hyperpolarized $^{13}C^{1}$. Acad Radiol 2006;13:932–942.
3. Golman K, in't Zandt R, Thaning M. Real-time metabolic imaging. Proc Natl Acad Sci USA 2006;103:11270–11275.
4. Kohler SJ, Yen Y, Wolber J, Chen AP, Albers MJ, Bok R, Zhang V, Tropp J, Nelson SJ, Vigneron DB, Kurhanewicz J, Hurd RE. In vivo 13 carbon metabolic imaging at 3T with hyperpolarized $^{13}C$-1-pyruvate. Magn Reson Med 2007;58:65–69.
5. Chen AP, Albers MJ, Cunningham CH, Kohler SJ, Yen YF, Hurd RE, Tropp J, Bok R, Pauly JM, Nelson SJ, Kurhanewicz J, Vigneron DB. Hyperpolarized C-13 spectroscopic imaging of the TRAMP mouse at 3T: initial experience. Magn Reson Med 2007;58:1099–1106.
6. Cunningham CH, Chen AP, Albers MJ, Kurhanewicz J, Hurd RE, Yen YF, Pauly JM, Nelson SJ, Vigneron DB. Double spin-echo sequence for rapid spectroscopic imaging of hyperpolarized $^{13}C$. J Magn Reson 2007; 187:357–362.
7. Albers MJ, Chen AP, Bok R, Zhang VY, Hurd RE, Yen YF, Zierhut ML, Nelson SJ, Vigneron DB, Kurhanewicz J. Monitoring prostate cancer progression in a transgenic murine model using 3T hyperpolarized $^{13}C$ MRSI. In: Proceedings of the 15th Annual Meeting of ISMRM, Berlin, Germany, 2007 (Abstract 367).
8. Nelson SJ, Chen AP, Bok R, Albers MJ, Zierhut ML, Kurhanewicz J, Vigneron DB, Kohler SJ, Yen YF, Tropp J, Gram KA, Wolber J, Dirven H, Hurd RE. Hyperpolarized C-13 MRSI data of dog prostate at 3T. In: Proceedings of the 15th Annual Meeting of ISMRM, Berlin, Germany, 2007 (Abstract 536).
9. Yen YF, Chen AP, Zierhut ML, Bok R, Zhang VY, Albers MJ, Tropp J, Nelson SJ, Vigneron DB, Kurhanewicz J, Hurd RE. EPSI sampling strategies for spectroscopic imaging of sparse spectra: applications for hyperpolarized $^{13}C$ imaging. In: Proceedings of the 15th Annual Meeting of ISMRM, Berlin, Germany, 2007 (Abstract 2928).
10. Ardenkjaer-Larsen JH, Fridlund B, Gram A, Hansson G, Hansson L, Lerche MH, Servin R, Thaning M, Golman K. Increase in signal-to-noise ratio of >10,000 times in liquid-state NMR. Proc Natl Acad Sci USA 2003;100:10158–10163.

11. Albers MJ, Bok R, Chen AP, Cunningham CH, Zierhut ML, Zhang VY, Kohler SJ, Tropp J, Hurd RE, Yen YF, Nelson SJ, Vigneron DB, Kurhanewicz J. Hyperpolarized $^{13}$C lactate, pyruvate, and alanine: noninvasive biomarkers for prostate cancer detection and grading. Cancer Res 2008;68:8607–8615.
12. Chen AP, Bok R, Zhang V, Xu D, Veeraraghavan S, Hurd RE, Nelson SJ, Kurhanewicz J, Vigneron DB. Serial hyperpolarized $^{13}$C 3D-MRSI following therapy in a mouse model of prostate cancer. In: Proceedings of the 16th Annual Meeting of ISMRM, Toronto, Ontario, Canada, 2008 (Abstract 888).
13. Zhao L, Mulkern R, Tseng C-H, Williamson D, Patz S, Kraft R, Walsworth RL, Jolesz FA, Albert MS. Gradient-echo imaging considerations for hyperpolarized $^{129}$Xe MR. J Magn Reson 1996;B113:179–183.
14. Mugler JP III. Optimization of gradient-echo sequences for hyperpolarized noble gas MRI. In: Proceedings of the 6th Annual Meeting of ISMRM, Sydney, Australia, 1998 (Abstract 1904).
15. Johnson GA, Cofer GP, Hedlund LW, Maronpot RR, Suddarth SA. Registered $^{1}$H and $^{3}$He magnetic resonance microscopy of the lung. Magn Reson Med 2001;45:365–370.
16. Wild JM, Paley MNJ, Viallon M, Schreiber WG, van Beek EJR, Griffiths PD. *k*-Space filtering in 2D gradient-echo breath-hold hyperpolarized $^{3}$He MRI: spatial resolution and signal-to-noise ratio considerations. Magn Reson Med 2002;47:687–695.
17. Svensson J, Petersson JS, Ståhlberg F, Larsson EM, Leander P, Olsson LE. Image artifacts due to a time-varying contrast medium concentration in 3D contrast-enhanced MRA. J Magn Reson Imaging 1999;10:919–928.
18. Mansfield P. Spatial mapping of the chemical shift in NMR. Magn Reson Med 1984;1:370–386.
19. Posse S, Gioacchino T, Risinger R, Ogg R, Le Bihan D. High speed $^{1}$H spectroscopic imaging in human brain by echo-planar spatial-spectral encoding. Magn Reson Med 1995;33:34–40.
20. Feinberg DA, Turner R, Jakab PD, von Kienlin M. Echo-planar imaging with asymmetric gradient modulation and inner-volume excitation. Magn Reson Med 1990;13:162–169.
21. Cunningham CH, Vigneron DB, Chen AP, Xu D, Nelson SJ, Hurd RE, Kelley DA, Pauly JM. Design of flyback echo-planar readout gradients for magnetic resonance spectroscopic imaging. Magn Reson Med 2005;54:1286–1289.
22. Derby K, Tropp J, Hawryszko C. Design and evaluation of a novel dual-tuned resonator for spectroscopic imaging. J Magn Reson 1990;86:645–651.
23. Zierhut ML, Yen YF, Chen AP, Bok R, Albers MJ, Zhang V, Tropp J, Park I, Vigneron DB, Kurhanewicz J, Hurd RE, Nelson SJ. How does dose of hyperpolarized $^{13}$C$^{1}$-pyruvate affect metabolic results in dog prostate? In: Proceedings of the 16th Annual Meeting of ISMRM, Toronto, Ontario, Canada, 2008 (Abstract 891).